JCI insight

Neuronal activity in vivo enhances functional myelin repair

Fernando C. Ortiz, … , Brahim Nait-Oumesmar, Maria Cecilia Angulo

JCI Insight. 2019. https://doi.org/10.1172/jci.insight.123434.

Research In-Press Preview Neuroscience

Graphical abstract

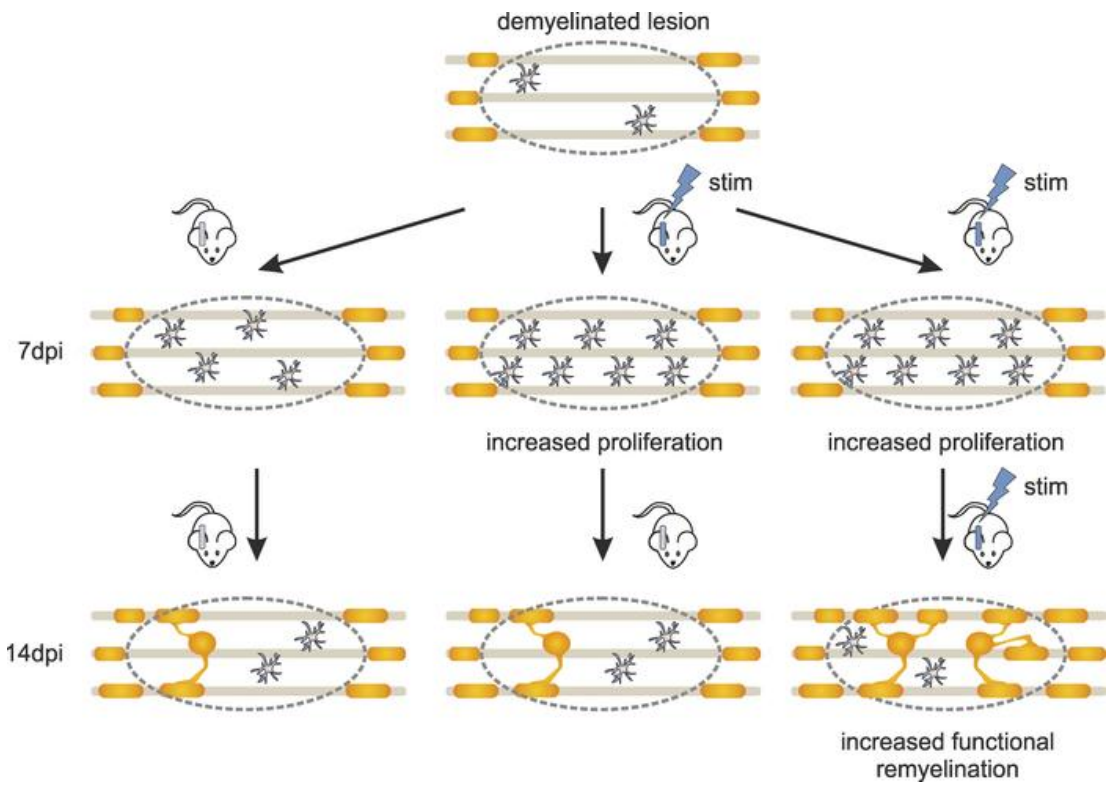

Neuronal activity in vivo enhances functional myelin repair

Fernando C Ortiz[1,2,6,7], Chloé Habermacher[1,2,3,7], Mariana Graciarena[4], Pierre-Yves Houry[1,2], Akiko Nishiyama[5], Brahim Nait Oumesmar[4], María Cecilia Angulo[1,2,3]*

[1] INSERM U1128, Paris, France

[2] Université Paris Descartes, Sorbonne Paris Cité, Paris, France

[3] Institute of Psychiatry and Neuroscience of Paris (IPNP), INSERM U1266, Paris, France

[4] Institut du Cerveau et de la Moelle épinière, Sorbonne Université, INSERM U1127, CNRS UMR 7225, Paris, France

[5] Department of Physiology and Neurobiology, University of Connecticut, Storrs, Connecticut, USA

[6] Instituto de Ciencias Biomédicas, Facultad de Ciencias de la Salud, Universidad Autónoma de Chile, Santiago, Chile

[7] These authors contributed equally to this work.

Conflict of Interests

The authors have declared that no conflict of interest exists.

Corresponding Author

María Cecilia Angulo, Center of Psychiatry and Neuroscience; INSERM U1266; Université Paris Descartes, Sorbonne Paris Cité; 102, rue de la Santé; 75014 Paris; FRANCE. Tel: 33-1-40789243. e-mail address: maria-cecilia.angulo@parisdescartes.fr

Abstract

In demyelinating diseases such as Multiple Sclerosis (MS), demyelination of neuronal fibers impairs impulse conduction and causes axon degeneration. While neuronal activity stimulates oligodendrocyte production and myelination in normal conditions, it remains unclear whether the activity of demyelinated axons restores their loss-of-function in a harmful environment. To investigate this question, we established a model to induce a moderate optogenetic stimulation of demyelinated axons in the *corpus callosum* at the level of the motor cortex in which cortical circuit activation and locomotor effects were reduced in adult freely moving mice. We demonstrate that a moderate activation of demyelinated axons enhances the differentiation of oligodendrocyte precursor cells onto mature oligodendrocytes, but only under a repeated stimulation paradigm. This activity-dependent increase in the oligodendrocyte pool promotes an extensive remyelination and functional restoration of conduction, as revealed by ultrastructural analyses and compound action potential recordings. Our findings reveal the need of preserving an appropriate neuronal activity in the damaged tissue to promote oligodendrocyte differentiation and remyelination, likely by enhancing axon-oligodendroglia interactions. Our results provide new perspectives for translational research using neuromodulation in demyelinating diseases.

Introduction

In Multiple Sclerosis (MS), impaired impulse conduction arises when immune-mediated demyelination destroys the myelin sheaths and causes the death of myelin-forming oligodendrocytes (OL) and progressive axon loss (1). However, production of newly formed OLs and some extent of myelin repair can occur in this demyelinating disease. Unfortunately, remyelination is often incomplete and ultimately fails in inducing functional recovery of patients with long-standing and progressive disease (1). Oligodendrocyte precursor cells (OPCs) are the main source of remyelinating OLs in demyelinated lesions. In some MS lesions populated by OPCs, remyelination fails probably because the cell microenvironment is highly perturbed and axons are poorly receptive for remyelination (2,3). Therefore, the mere presence of OPCs in a lesion is insufficient to stimulate a regenerative process. Importantly, neuronal activity is critical for the regulation of OPC proliferation, differentiation and myelination in the normal central nervous system (CNS) (4-10). Although the effect of neuronal activity on remyelination has been less studied, it could also be a key external factor in enhancing myelin regeneration. A role of neuronal activity in endogenous remyelination is suggested by the effect of in vivo perfusion of the Na+ channel blocker tetrodotoxin (TTX) which increases the density of proliferating OPCs and reduces remyelination in a context of acute toxin-induced demyelinated lesions (11). However, whether and which pattern of activity of demyelinated axons in its adverse cellular environment could have a beneficial effect during myelin regeneration is unknown.

If neuronal activity is critical to support remyelination, increasing the activity of demyelinated axons should improve this process. In cell cultures, low-frequency electrical stimulation of dorsal root ganglion (DRG) axons is associated with reduced number of myelin segments (12), while increasing the stimulation to physiological firing rates for DRG

neurons reduces OPC proliferation favoring their differentiation onto myelinating OLs (13). Under normal in vivo conditions, however, distinct and sometimes contradictory effects of neuronal activity have been described. The most accepted notion is that neuronal stimulation in freely moving mice induces a rise in OPC proliferation that is followed by their differentiation into newly-generated OLs (6,7,9,14). However, different intensities, frequencies and durations of neuronal activity in distinct in vivo preparations can also: 1) trigger OPC differentiation without a prior proliferative process (14), 2) shift the balance towards more OPC proliferation (6), or 3) lead to no changes in the number of cycling OPCs (9). Considering these variable results in normal conditions, it is thus difficult to predict which activity pattern of demyelinated fibers could promote OL differentiation and myelin repair in pathological conditions.

To investigate whether neuronal activity can enhance oligodendrocyte differentiation and restore myelin regeneration in demyelinated lesions, we established a model to stimulate demyelinated fibers using an optogenetic-based approach in freely moving mice after a lysophosphatidylcholine (LPC)-induced focal demyelination of *corpus callosum* at the level of the motor cortex. We adjusted the stimulation parameters to obtain a restricted neuronal activation that does not cause changes in motor behavior but trigger action potentials in demyelinated axons. We studied the impact of neuronal activity in modulating different stages of remyelination by analyzing OPC proliferation and differentiation, the extent of myelin regeneration and the functional recovery of the fibers. We found that, after an acute demyelination, neuronal activity in vivo enhances the differentiation of OPCs onto myelinating OLs inducing a remarkable ultrastructural and functional improvement, but only under a repeated stimulation paradigm. Our results highlight the importance to preserve a

controlled, moderate and recurrent activity of demyelinating axons to improve myelin regeneration.

Results

Model for moderate optogenetic stimulation of demyelinated callosal fibers in vivo

In Thy1-ChR2-YFP mice, layer V pyramidal neurons of the neocortex selectively express the light-sensitive channel channelrhodopsin-2 (ChR2) fused to YFP under the Thy1 promoter (15). In the motor cortex, these neurons are highly myelinated thus conveying rapid information outside this region (16) and directly contributing to the execution of voluntary movements. In line with this, their optogenetic stimulation with an optic fiber placed at the pial surface in freely moving mice triggers a locomotor behavior during blue light stimulation trains characterized by circular stereotyped displacements and sometimes followed by epileptic-like seizures (6) (Supplemental Figure 1). This stimulation provides a broad activation of neuronal circuits involved in locomotor behavior. Changes in motor activity constitute a convenient readout to assess the efficiency of photostimulation in normal conditions (Supplemental Figure 1). However, this wide neuronal network activation seems less suitable to study local repair mechanisms since its off-target effects alter both global circuit functioning and animal behavior.

Here we performed LPC-induced demyelinated lesions in *corpus callosum* of adult Thy1-ChR2-YFP mice at the level of the motor cortex. To avoid a wide activation of motor circuits and ensure the targeting of demyelinated axons inside LPC-induced lesions, we implanted a mini-optic fiber that extended to deep cortical layers and which tip laid above LPC-induced lesions (Figure 1A). Contrary to the stimulation at the pial surface (Supplemental Figure 1), we found that unilateral 30 s-light pulse trains delivered at 20 Hz every 4.5 min did not induce modifications in locomotor behavior when comparing stimulated and non-stimulated (control) mice over 50 min (10 trains; Figure 1B, C).

Furthermore, no significant changes were observed when analyzing 30 s periods before, during and after each stimulation train (Figure 1D; $p>0.05$ for turning tendency, traveled distance and mean speed, respectively, analyzed for 10 consecutive trains, two-way ANOVA followed by a Bonferroni's multiple comparison; n=5 mice). In the absence of behavioral changes, we verified that the stimulation was efficient by implanting an optrode accommodating a recording electrode inside the demyelinated lesion. Light-evoked local field potentials (LFPs) were recorded for each light pulse of 10 ms in long trains up to 30 s in anesthetized Thy1-ChR2-YFP mice, but were absent in wild-type mice (Figure 1E; Supplemental Figure 2A, B). We also confirmed that layer V pyramidal neurons in acute cortical slices triggered action potentials with high fidelity during 30 s stimulation trains at 20 Hz, a frequency compatible with their averaged firing rate in the motor cortex (17) (Supplemental Figure 2C, D).

After in vivo light stimulation, LPC-induced lesions were recognized in brain tissue sections by the lack of myelin basic protein (MBP) immunostaining (Figure 1F). Only lesions showing demyelinated YFP^+ axons were kept for analysis to avoid those with a potential mechanical damage induced during LPC injection (Figure 1F). Although the size of the lesions and number of cells expressing the oligodendroglia cell lineage marker Olig2 was very variable (Supplemental Figure 3A-C), the $Olig2^+$ cell density was constant among lesions allowing for comparative analysis between conditions (Supplemental Figure 3D). Altogether, these results validate our in vivo model for moderate optogenetic stimulation of demyelinated ChR2-expressing axons in LPC-induced lesions without causing major behavioral locomotor changes.

A photostimulation session leads to a rapid increase in the OPC pool inside demyelinated lesions

Since the LPC-induced demyelination model elicits a synchronized and successive response of OPCs and OLs (18,19), the effect of increased neuronal activity can be evaluated at different stages of the demyelination/remyelination processes. We first assessed the effect of an increased demyelinated axon activity on OPC density after a single photostimulation session at 7 dpi, a time point which corresponds to the tail end of OPC proliferation and the beginning of OPC differentiation that is expected to occur spontaneously in the absence of photostimulation (18,19). Mice were photostimulated for 3 h with 10 ms light pulses applied at 20 Hz during 30 s every 4.5 min and perfused 1h after the end of photostimulation (Figure 2A). A triple immunostaining was performed to simultaneously identify the lack of myelin in lesions of *corpus callosum* (MBP), all OL lineage cells (Olig2) and mature OLs (CC1). We considered $Olig2^+/CC1^-$ cells as OPCs and $Olig2^+/CC1^+$ cells as differentiated OLs (Figure 2B). We found a 1.61-fold increase of OPC density in photostimulated lesions compared to control lesions while no differences were observed in OL density (Figure 2C). Consistent with previous findings in normal conditions (Gibson et al., 2014), the increased OPC density in the ipsilateral side was not accompanied by changes in OPC or OL populations in the contralateral side (Supplemental Figure 4A). In addition, we observed that only 1.28±0.77% of $Olig2^+$ cells co-express the astrocytic marker GFAP in photostimulated lesions (n= 5, not shown), confirming that the observed cell density increase was restricted to the OPC population. Our results show that a transient increase in the activity of demyelinated axons is sufficient to rapidly raise the OPC density inside demyelinated lesions.

Several reports have shown that, during normal myelination, neuronal activity increases the number of cycling OPCs as revealed by 5'-ethynyl-2'-deoxyuridine (EdU)

staining that labels proliferative cells in the S phase of the cell cycle (6,9,14). By performing two injections of EdU at the beginning and at the end of the photostimulation session (Figure 2A), we explored whether a similar cellular mechanism could explain the rapid activity-dependent increase of OPC density in demyelinated lesions at 7 dpi. First, we found that most of EdU^+ cells were $Olig2^-$ in control and photostimulated lesions and did not display any density change upon phtotostimulation (Figure 2E). Although no changes were observed for these proliferative cells that should mainly comprise astrocytes and microglia, neuronal activity could affect independently each of these populations. We therefore performed specific experiments to follow proliferative microglia and astrocytes inside lesions (Supplemental Figure 5). No differences were observed on the EdU^+/IBA1+ micrgolia or $EdU^+/GFAP^+$ astrocyte densities between control and phostostimulated mice, indicating that neuronal activity does not significantly affect the proliferation of these cell types in lesions (Supplemental Figure 5B, D). On the contrary, we observed a 2.83-fold increase in the number of $EdU^+/Olig2^+$ cells in photostimulated mice compared to controls (Figure 2E, bottom). To rule out that this increase in OPC proliferation was due to a non-specific effect of tissue heating by light, we compared the density of proliferative cells in lesions of photostimulated wild-type mice with those of non-photostimulated Thy1-ChR2-YFP mice. No changes in $EdU^+/Olig2^-$ or $EdU^+/Olig2^+$ cell densities were observed between these two conditions, showing that the rise of OPC proliferation is due to the increased neuronal activity (Supplemental Figure 4B). Altogether, these results indicate that the activity of demyelinated axons induced by light stimulation specifically enhances the available OPC pool inside the lesion by increasing their proliferation rate in an activity-dependent manner.

A repeated photostimulation protocol is required to enhance OL differentiation in LPC-induced lesions

During the second week following the LPC injection, a massive differentiation of OPCs onto OLs commonly occurs (18,19). We thus tested whether the increased OPC pool generated by a single photostimulation session at 7 dpi was able to produce more differentiated OLs a week later (Figure 3A, top). However, OPC and OL densities were unchanged between control and single photostimulated lesions at 14 dpi (Figure 3B, C), suggesting that the exceeding OPC pool induced by neuronal activity at 7 dpi was unable to generate mature OLs. To track the proliferative OPC population during the first days following photostimulation, we performed four EdU injections per day from 7 dpi to 10 dpi and analyzed the densities of $EdU^+/Olig2^+/CC1^-$ OPCs and $EdU^+/Olig2^+/CC1^+$ OLs in control and photostimulated mice (see Methods). Despite a large number of EdU^+ cells stained with this protocol, only a minimal fraction corresponded to $EdU^+/Olig2^+/CC1^+$ OLs in both conditions (Supplemental Figure 6). Moreover, no changes were obtained either for EdU^+ cells or the total number of OPCs and OLs between photostimulated and non-photostimulated mice (Supplemental Figure 6C, D). These results indicate that the OPC pool generated in an activity-dependent manner at 7 dpi was little differentiated into OLs few days later. They also suggest that this pool disappeared within 3 days following the increase in neuronal activity. The rise of OPC density induced by a single photostimulation session at 7 dpi is therefore insufficient to produce long-term modifications in the oligodendroglia population during a week of highly dynamic cellular changes in the demyelinated lesion (18,19,20).

Considering the transient effect of a single photostimulation session on OPCs, we reasoned that to maintain the new OPC pool induced by neuronal activity at 7 dpi and provoke its development onto mature OLs, it could be necessary to repeat the 3h-photostimulation protocol every day during the critical period of OPC differentiation, *i.e.* between 7 dpi and 13 dpi (Figure

3A, bottom). In line with this postulate, a repeated photostimulation protocol induced a 1.67-fold increase in the number of mature OLs without causing clear changes in OPC density at 14 dpi (Figure 3B, C). This OL density increase was not accompanied by a change in the total $Olig2^+$ cell density (1112±98, 1039±92 and 1285±67 cells per mm^2 for control, single and repeated photostimulation, respectively; $p>0.05$, K-W st.=3.665, Kruskal-Wallis Test followed by a Bonferroni's multiple comparison). Thus, while a single session of neuronal activity only transiently affects the OPC population in demyelinated lesions, a recurrent neuronal activity for a week is needed to maintain the new OPC pool and promote OPC differentiation, resulting in a significant increase of the population of mature OLs.

A repeated neuronal activity of demyelinated axons in vivo promotes myelin repair and functional recovery

Our repeated photostimulation of demyelinated axons leads to an increased pool of OLs inside LPC-induced lesions (Figure 3B, C). However, an increased number of OLs does not necessarily imply that more newly-formed compact myelin will be generated under pathological conditions. To determine whether remyelination is improved after a repeated photostimulation, we performed transmission electron microscopy (EM) analyses of normal appearing white matter (NAWM), control lesions and repeated photostimulated lesions at 14 dpi (Figure 4A) and quantified remyelinated axons distinguished by their thinner myelin and their decreased myelin optical density profiles (Figure 4B and Supplemental Figure 7A-C). As expected, axons with thin myelin sheaths, indicative of remyelinated axons (1), were detected in demyelinated lesions at 14 dpi but very few were seen in NAWM (Figure 4A, B). On the contrary, EM analysis revealed a 2.02-fold increase of remyelinated axons in

photostimulated lesions compared to control lesions, indicating that a recurrent neuronal activity stimulates myelin regeneration (Figure 4A, B).

Then, we calculated the g-ratio of randomly selected axons to evaluate the myelin sheath thickness with respect to axon diameter in each condition (Figure 4C). We found that the g-ratio distributions were significantly different among the three tested conditions (Figure 4C). This difference was not explained by changes in axon size in lesions of control and after repeated photostimulation mice since axon diameters distributions were not modified with respect to NAWM (Supplemental Figure 7D). However, we observed that the slope of the g-ratio relative to axon diameter after repeated photostimulation was significantly different to that of both NAWM and control lesions (Figure 4D), suggesting that the increased remyelination resulting from a repeated photostimulation did not equally occur in demyelinated axons of different size. In fact, for axons displaying a diameter smaller than 0.793 µm, which corresponded to the intersection of linear fits for control lesions and repeated photostimulation conditions, the myelin thickness was almost identical in control lesions compared to photostimulated mice, but different to NAWM (Figure 4D; g-ratio: 0.741±0.003, 0.753±0.004 and 0.766±0.005 for NAWM, control lesions and repeated photostimulated; K-W st.= 27.79, p=0.411 for repeated *vs* control, p<0.0001 for NAWM *vs* control, p=0.0001 for repeated *vs* NAWM; Kruskal-Wallis Test followed by a Bonferroni's multiple comparison). On the contrary, for axons displaying a diameter larger than 0.793 µm, the g-ratio of repeated photostimulation and NAWM conditions were similar, but significantly smaller compared to control (Figure 4D; g-ratio: 0.830±0.002, 0.843±0.003 and 0.830±0.001 for NAWM, control lesions and repeated photostimulated; K-W st.= 43.73, p=1.0 for repeated *vs* NAWM, p<0.0001 for both repeated *vs* control and NAWM *vs* control; Kruskal-Wallis Test followed by a Bonferroni's multiple comparison). These findings

indicate that the enhanced remyelination promoted by a repeated neuronal activity is biased towards larger diameter axons. However, it is not biased towards ChR2-expressing axons since the proportion of myelinated YFP+ axon segments with respect to the total myelinated axon segments did not change between control and photostimulated mice (Supplemental Fig. 7E, F).

To assess whether the activity-dependent enhanced remyelination was accompanied by a functional improvement of conduction in photostimulated mice, we recorded evoked compound action potentials (CAPs) in acute coronal slices of *corpus callosum* at 14 dpi after performing in vivo experiments (Figure 3A, bottom). The demyelinated area was recognized as a brighter region surrounding white matter (Supplemental Figure 2B). In the normal *corpus callosum* (NAWM), CAPs were characterized by the presence of a fast and slow component corresponding respectively to myelinated and unmyelinated axon responses (21) (Figure 5A). As expected in control demyelinated lesions, the fast component was highly reduced or disappeared (Figure 5A). However, the increase in remyelination after repeated photostimulation induced a recovery of the fast component, which had the same conduction velocity than NAWM (Figure 5A, B). Moreover, the normalized area-under-the-curve (AUC) of the fast component was smaller in control but reached normal values after repeated photostimulation (Figure 5B). Finally, comparison of normalized CAP amplitudes revealed that the fast component was significantly reduced in control lesions with respect to NAWM but rescued in photostimulated mice (Figure 5B). Altogether, these experiments indicate an extensive ultrastructural and functional recovery of demyelinated fibers upon a repeated photostimulation of demyelinated axons in vivo.

Discussion

This report demonstrates that a moderate and controlled neuronal activity in vivo increases the pool of mature OLs, enhances remyelination and restores action potential conduction in demyelinated lesions. We also show that the recurrence with which the lesion is stimulated constitutes an important factor to take into account. While a single episode of activity has only a transient effect on the OPC population, a recurrent activity promotes a robust increase in OL density and enhances remyelination. Therefore, neuronal activity is able to enhance OPC differentiation and myelin synthesis in an altered environment as a demyelinated lesion. Remyelinated injured axons, in turn, undergo a significant functional recovery.

Recent studies have demonstrated that neuronal activity promotes oligodendrocyte differentiation in the healthy brain, but the cellular mechanisms responsible for this effect are not completely clear. A transient 30 min photostimulation of ChR2-expressing motor neurons was sufficient to increase OPC proliferation followed by a later more modest rise in the OL population in the neocortex and *corpus callosum* (6). On the contrary, a single DREADD-mediated neuronal stimulation did not cause modifications in the number of cycling OPCs in *corpus callosum* at the level of the somatosensory cortex (9). Seven days of sustained stimulation using a DREADD approach were needed to induce OPC proliferation and a subsequent differentiation of newly-divided OPCs into myelinating OLs (9). Although understanding the causes of the different cellular responses of OL lineage cells to neuronal activity is not straightforward, substantial differences exist among studies. In Gibson et al. (2014), the optogenetic stimulation specifically targeted layer V pyramidal neurons, while in Nagy et al. (2017) and Mitew et al. (2018), the number and selectivity of stimulated fibers were probably more heterogeneous since the fibers recruited during electrical stimulation and

the efficiency of *in utero* electroporation, respectively, are variable. Finally, the dynamics of both OPCs and OLs can be easily manipulated by experience and injury in young mice (22,23). Although experience-dependent enhancement of OL production and myelination in the mature cortex also occurs (24), the activity-dependent OPC plasticity declines with age (9). Therefore, different preparations, animal ages and stimulation paradigms including various intensities, frequencies and durations probably cause different effects (14). In this context of complex cellular responses, it was unknown whether the activity of demyelinated axons in lesions, where environmental factors causing the damage radically change the conditions, could have a positive effect on remyelination. We show that a single photostimulation session at 7 dpi in the adult induces a rapid increase in the OPC population. As in Gibson et al. (2014), this rapid rise in OPC density is probably caused by an increment in the proliferative fraction. However, the OPC density increase at 7 dpi was not associated with an increased number of OPCs and mature OLs three days or one week after a single episode of increased neuronal activity. This transient rise in the OPC pool suggests that, in the absence of increased activity, the survival of an exceeding number of OPC inside the lesion is compromised. Although this apparently homeostatic response needs further investigation, our findings clearly show that a recurrent but moderate neuronal activity during a week was needed to maintain the OPC pool and induce its differentiation into myelinating OLs. Thus, recurrent photostimulation probably shifts the balance from OPC proliferation towards more differentiation. This process could also act in conjunction with an activity-dependent pro-survival effect (22,24). Collectively, these data provide evidence for the existence of different responses of oligodendrocyte lineage cells to neuronal activity that may vary according to the number and type of stimulated fibers, the frequency and patterns of

stimulation, the neurotransmitter and signaling molecules release during neuronal activity, the age of the animals and physiological *versus* pathological conditions.

The concept of activity-driven adaptive myelination represents an important recent advance in our understanding of the myelination process (25). However, the molecular mechanisms linking neuronal activity with oligodendroglia development and myelin production remain poorly understood. Since axon-oligodendroglia interactions induce OPC differentiation (10,26) and myelin formation (8,10,27), it is conceivable that neuronal activity directly triggers molecular changes in OPCs and OLs. These glial cell types express different synaptic and extrasynaptic receptors for neurotransmitters according to their developmental state (28). An interesting possibility is therefore that neurons displaying different levels of activity and/or cell identities activate distinct neurotransmitter receptors on oligodendroglia that, in turn, modulate the expression of transcription factors and epigenetic regulators involved in OPC maturation and OL myelin production. Other factors released by neurons such as brain-derived neurotrophic factor (BDNF), neuregulin or fractalkine may also be released in an activity-dependent manner to promote OPC differentiation and myelination (29,30,31). Alternatively, astrocytes and microglia could indirectly contribute to activity-driven adaptive myelination. For instance, enhanced neuronal activity in cell cultures promotes myelination through ATP-dependent secretion of leukemia inhibitory factor (LIF) from astrocytes (32). In addition, astrocytes and microglia release different soluble factors that, in demyelinated conditions, have either detrimental or beneficial effects on OPC fate and myelin repair (20,33). Further investigations are needed to understand whether neuronal activity influences the release of these factors and mediates glia-oligodendroglia interactions in normal and pathological conditions.

Whether myelin sheaths on remyelinated axons also display activity-dependent plasticity was still an opened question (1). Our study demonstrates that recurrent stimulation of demyelinated fibers not only modifies oligodendroglia behavior inside lesions, but also induces an impressive improvement in functional remyelination. Hence, the process of myelin repair in demyelinated lesions is also plastic, although differences between physiological and pathological conditions exist. During development, more neuronal activity results in thicker myelin sheaths with a global decreased g-ratio (6,9). Following demyelination, however, we did not observe thicker remyelinated axons after repeated photostimulation compared to NAWM. In a first approach, we found that a recurrent neuronal activity induces a 2-fold increase in the number of axons undergoing remyelination as revealed by their thinner myelin. This increase probably represents an underestimation of the number of remyelinated axons if we considered that, in these countings, we did not take into account those axons displaying near-normal myelin in the lesion. Indeed, further EM analysis performed in randomly selected axons showed that the activity-dependent myelin formation appears biased towards axons with diameters larger than 0.793 µm for which the averaged g-ratio reached the value obtained for NAWM. In addition, the g-ratio distribution changed from a bimodal in both control lesions and NAWM to a single Gaussian after repeated photostimulation (Figure 5C), suggesting that the evoked activity of layer V pyramidal axons induces a preferential phenotype of axon remyelination. Although we observed an effect biased towards larger axons, we cannot totally rule out that an enhanced activity-dependent remyelination occurs in both small and large axons, but with larger axons displaying a proportionally thicker myelin sheath and thus, a smaller g-ratio. Indeed, we did not observe a preferential myelination of ChR2-expressing YFP^+ axons which largely belongs to layer V pyramidal cells known to display large diameter axons (16). In any case, if

myelin was thicker in larger diameter axons, this would imply that remyelination of those axons was of better quality than that of smaller ones, probably because many of them were ChR2-positive and thus activated by light. Moreover, we observed that repeated photostimulation was accompanied by a full recovery of the conduction velocity of CAPs measured inside the lesion (Figure 5). This full recovery is in agreement with the fact that CAP measurements are biased to account mostly for the activity of larger diameter axons (34,35). Indeed, CAP recordings are a robust but also an inhomogeneous averaged way to measure the conduction of a diverse axon population (35). Nevertheless, our data show that activity extensively improves remyelination and conduction, a repairing process that should be beneficial to protect axons from degeneration (36).

It was recently showed that pharmacological therapies with drugs known to stimulate OL differentiation constitute a possible approach in demyelinating diseases (37). This finding emphasizes the importance of understanding the biological basis for a successful endogenous remyelination, a necessary condition to identify effective strategies enhancing myelin repair. An important first step to achieve this goal is to know the intrinsic and extrinsic factors that modify the oligodendroglia genesis and fate as well as the sequence of events in which these factors act (38). Our study is the first to demonstrate a strong remyelinating effect of neuronal activity in vivo and establish the conditions in which this activity is highly efficient in pathological conditions. Our findings provide the proof-of-concept for new clinical trials aiming at testing the therapeutic efficacy of either electrical or chemical neuromodulation. Clinical studies have already explored neuromodulation as a possible treatment for demyelinating diseases such as MS (39). Thalamic Deep Brain Stimulation (DBS) in MS patients has shown improvements in the typically associated tremor (40,41) and ameliorates the neuropathic pain of MS-induced trigeminal neuralgia (42). Likewise, repetitive

transcranial magnetic stimulation (rTMS) of the motor cortex improved some of the associated symptoms in MS patients, such as spasticity and cerebellar dysfunction (43,44,45). However, despite the potential beneficial effects of these approaches, available data are still sparse and sometimes contradictory (39,46). Our results establish fundamental cellular principles of how the activity of demyelinated axons, when they still have the capacity to drive action potentials, leads to changes in OL lineage cell dynamics promoting oligodendrocyte differentiation and improving functional remyelination in the damaged tissue. Our work supports the notion that activity-dependent myelin repair of the CNS can be achieved after a demyelinating injury and open new promising avenues for early therapeutic intervention to enhance myelin regeneration in demyelinating diseases, such as MS.

Methods

Animals and Surgery

Experiments were performed with heterozygous male and female C57/BL6 Thy1-ChR2-YFP transgenic adult mice (8-9 weeks old) obtained from The Jackson Laboratories (stock N° 007612) (15) and backcrossed for more than 10 generations. Few experiments were also performed using male and female C57/BL6 wild-type mice of the same age.

For inducing a focal demyelinating lesion, mice were deeply anesthetized with ketamine/xylazine (0.1/0.01 mg/g, IP) and fixed in a stereotaxic frame (Kopf Instruments). Ophtalmic Dexpanthenol gel (Chauvin Bausch & Lomb GmbH) was applied to the eyes to prevent dehydration. The skin above the skull was disinfected and incised. Then, a hole was stereotaxically drilled on the motor cortex area to allow a glass pipette connected to a Hamilton syringe to be lowered into *corpus callosum* in order to inject 2 µl of lysophosphatidylcholine (LPC, Sigma, 1% in PBS), as we previously described (coordinates: 1 mm lateral to midline, 1.5 mm anterior to Bregma, and 1.8 mm depth from brain surface) (19).

For optogenetic stimulation, the same hole used for LPC injections was employed to implant a cannula accommodating a mini-optic fiber (cannula: 1.25 mm; fiber: 200 µm diameter, numerical aperture=0.66; Prizmatix Ltd., Israel). This manipulation was performed ten minutes after LPC injections during the same surgery. The mini-optic fiber was stereotaxically lowered into deep layers of the motor cortex, above the injected *corpus callosum* (fiber: 1.4 mm protrusion). Then, the optogenetic implant was fixed to the skull with dental cement (Unifast Trad ivory 339104) (Figure 1A). Finally, the skin was sutured

(Mersilene®, EH7147H, Ethicon) around the implant. Mice were recovered from anesthesia in an environment at 37°C before they returned to their home cages.

Photostimulation and local field potential (LFP) recordings in vivo

The day of the photostimulation, the mini-optic fiber was connected to a 460 nm LED source through an optic fiber patch cord (Prizmatix). The LPC-induced demyelinated area was photostimulated in freely moving mice following a 3h protocol composed by 36 light trains of 30 s delivered at 20 Hz (10 ms on/40 ms off pulses) and separated by a resting period of 4.5 min. The power at the tip of each mini-optic fiber was systematically checked with an optical power meter (PM100D coupled with sensor S120C, Thorlabs) before surgery and set at ~1 mW the day of the experiment. Mice were randomly allocated to three different experimental groups that follow: 1) a single 3h photostimulation session at 7 dpi (single); 2) 3h photostimulation session repeated every day from 7 to 13 dpi (repeated); and 3) no photostimulation session but subjected to the same surgical procedures and connected to the optic fiber patch cord (control).

To confirm that demyelinated fibers inside LPC-induced lesions displayed neuronal activity upon in vivo photostimulation, a set of experiments was performed with a custom-made optrode built by assembling to the mini-optic fiber a recording electrode which tip reached the core of the demyelinated lesion (Ni/Ag wire, 50 µm diameter; ~1.6 mm length from the surface). The optrode was implanted and fixed to the mouse skull as described above. A pin connector was also fixed to the skull surface at the contralateral hemisphere and used as a ground for in vivo recordings (coordinates: 1 mm caudal and lateral to lambda). LFP recordings were obtained in anesthetized mice (ketamine/xylazine 0.1/0.01 mg/g) after connecting the optrode to both the pre-amplifier and the 460 nm LED source system. Light

trains from 1 s to 30 s delivered at 20 Hz were applied (1 mW; 10 ms light pulses), while light-evoked LFPs were recorded in current-clamp (I=0) voltage-follower mode. To confirm that LFPs were induced by the activation of ChR2+ fibers in lesions, the same experiment was performed in wild-type mice (negative controls). All electrophysiological data of this study were acquired at 20 KHz by using a Multiclamp 700B amplifier, filtered at 4 KHz, digitized with a digidata 1440 A and analyzed off-line with Pclamp10.1 software (Molecular Devices) and IgorPro 6.0 environment (Wavemetrics).

Open field behavior

Freely moving mice were video-recorded during photostimulation by using a CMOS camera (DFK22AUC03, Imaging Source) positioned above of a standard open-field box. Mouse behavior was monitored and analyzed by Smart video tracking software (version 3.05.05, PanLab). Light pulse delivery was coordinated with the video-acquisition by a TTL pulse controller (Pulser software, Prizmatix). To investigate motor behavior changes during photostimulation, we compared the turning tendency, the mean speed (with or without resting time) and the total traveled distance for 50 min video-recordings between photostimulated and control groups. We also analyzed these parameters before (30 s), during (30 s) and after (30 s) a train (for 10 trains).

Electrophysiology in acute brain slices

Acute coronal slices of LPC-injected *corpus callosum* (300 µm) were obtained from Thy1-ChR2-YFP transgenic adult mice (8-9 weeks old) as previously described (19). Slices were placed in a recording chamber perfused with a standard extracellular solution (3 mL/min) containing (in mM): 126 NaCl, 2.5 KCl, 1.25 NaH_2PO_4, 26 $NaHCO_3$, 20 glucose, 5

pyruvate, 3 $CaCl_2$, and 1 $MgCl_2$ (pH: 7.43; 95% O_2, 5% CO_2). For whole-cell recordings, layer V cortical YFP+ pyramidal neurons were visualized by fluorescence and DIC videomicroscopy, and recorded with a patch pipette using an intracellular solution containing (in mM): 120 K-gluconate, 5 NaCl, 3 MgCl2, 0.2 EGTA, 10 HEPES, 0.3 Na-GTP, 4 Na-ATP and 10 Na-phosphocreatine (pH 7.3, 295 mOsm). Light-evoked action potential discharges of YFP+ pyramidal neurons were elicited by light trains of different duration and delivered through an optic fiber placed above the patch pipette (fiber: 200 µm diameter, numerical aperture=0.53, power: 1 mW; Prizmatix).

For recordings of compound action potentials (CAPs), demyelinated lesions were recognized under the microscope as a brighter area in *corpus callosum* (Supplemental Figure 2B). CAPs were obtained by stimulating white matter fibers with a monopolar electrode placed outside the lesion, while the recording electrode (glass pipettes) was placed in the lesion core (60 V; 100 µs stimulations; Iso-Stim 01D, npi elec-tronic GmbH, Tamm, Germany). To calculate the conduction velocity, stimulation pulses were delivered at two different positions with respect to the recording electrode. The amplitudes of fast and slow components, the AUC and the conduction velocity were analyzed using acute slices of repeated stimulated and control demyelinated mice, as we previously described (21). CAPs were also measured in NAWM for comparison. For a more reliable comparison, the three conditions (NAWM, control, repeated) were tested the same day with the same stimulation and recording electrodes (n=3 mice per condition).

Immunostainings, EdU proliferation assays and countings

Animals were perfused intracardially with phosphate buffer saline (PBS) followed by 0.15 M phosphate buffer (PB) containing 4% paraformaldehyde (PFA, Electron Microscopy

Sciences), pH 7.4. For experiments at 7 dpi, mice were perfused 1h after the end of the 3h protocol. For experiments at 14 dpi, mice were perfused one day after the end of the last 3h protocol. After perfusion, brains were kept 1h in PFA and stored in PBS at 4°C before cutting. Sagittal vibratome slices (120 µm) were prepared in PBS at 4°C and permeabilized with 1% Triton and 4% Normal Goat Serum (NGS) during 2h.

Immunostainings against Olig2, CC1 and MBP were performed with rabbit anti-Olig2 (1:400, ref. AB9610, Merck-Millipore), mouse monoclonal anti-CC1 (1:100, ref. OP80, Calbiochem) and rat monoclonal anti-MBP (1:100, ref. AB7349, Abcam) diluted in 0.2% Triton X-100 and 4% NGS. Slices were first incubated with primary anti-Olig2 and anti-CC1 antibodies for 3 nights and revealed for 2h at RT with secondary antibodies coupled to Alexa-405 and Alexa-633, respectively (1:500, ThermoFisher Scientific). Next, the same slices were incubated with the primary anti-MBP antibody one more night and revealed for 2h at RT with a secondary antibody coupled to Alexa-555 (1:500, ThermoFisher Scientific). Negative controls were performed by omitting all primary antibodies or by incubating a primary antibody with a secondary antibody against an omitted primary antibody.

To label cells in the S phase of the cell cycle, we performed intraperitoneal EdU injections at 7 pdi (ref. C10340, ThermoFisher Scientific). In a first protocol, mice were injected 10 min before and after the 3h protocol (50 mg/kg per injection) at 7 dpi and perfused 1h later. Slices of EdU treated mice were first immunostained with either rabbit anti-Olig2 and rat anti-MBP or rat anti-MBP, rabbit anti-IBA1 (1:1000, ref. 019-19741, Wako), mouse anti-GFAP (1:100, ref. G3893, SIGMA). In a second protocol, mice were injected four times per day each 3h from 7 dpi to 10 dpi (20 mg/kg per injection) and perfused 1h after the last injection. In this case, slices of EdU treated mice were immunostained with rabbit anti-Olig2, mouse anti-CC1 and rat anti-MBP as described above.

EdU was revealed after immunostainings by using the Clik-iT EdU Alexa-647 (ref. C10340, ThermoFisher Scientific).

Confocal images were mainly acquired using a 20X (NA=0.8; 1.5 µm z-step) and 63X (NA=1.4; 0.75 µm z-step) oil objectives (NA=0.8 and 1.4, respectively) with LSM 710 confocal microscope (Zeiss) and processed using NIH ImageJ as described (47). For the analysis of the proportion of myelinated YFP^+ fibers in control and photostimulated mice, we used a 93X glycerol objective (NA=1.3; 0,35 µm z-step) mounted in a SP8 Leica confocal microscope, and quantified myelinated fiber segments as we previously described (47) in images of 62.5X62.5 μm^2 of 25 Z-sections. LPC-induced lesions were identified by the lack of MBP expression with a 20X objective and imaged for cell countings with a 63X oil objective. The lesion area was identified by the lack of MBP expression and delimited manually before cell countings. It is noteworthy that some degree of remyelination already occurred at 14 dpi, but the MBP staining was still sufficiently lower inside the lesion compared to a normal *corpus callosum* to delineate the lesion. Cell densities were obtained by counting OPCs and OLs with the ROI manager tool (ImageJ) and by dividing the number of cells by the defined demyelinated area.

Transmission electron microscopy

For ultrastructural visualization of myelinated axons, mice at 14 dpi were perfused with 5% glutaraldehyde and 4% PAF in PB 0.1M, pH 7.4. Brains were removed and immersed in the same solution for 1 hour. After rinsing brains with PB, 100 µm sagittal sections spanning the entire lesion area were obtained with a vibratome (Leica VT1000S), and subsequently incubated in 2% osmium tetroxide (OsO4) for 1 hour. Then, sections were rinsed in distilled water and contrasted with uranyl acetate 5% for 30 min. Samples were

dehydrated in a graded series of ethanol and cleared in acetone. Sections were then embedded in epoxy resin (Agar scientific, UK) and incubated at 56°C for 48h to allow for polymerization. Once polymerized, blocks were observed at the dissection microscope and the lesion area was manually microdissected. Dissected blocks were first cut in 1 µm semi-thin sections with an ultramicrotome (UC7, Leica). Sections were picked up every µm and stained with toluidine blue. Semi-thin sectioning was performed until the lesion area was observed. Then, serial ultra-thin sections (70 nm thick) were collected onto copper grids (about 3-4 sections per grid) and visualized at the transmission electronic microscope (Hitachi HT7700). Electron micrographs from the lesion areas were taken at ×18 000 magnification, using an integrated AMT XR41-B camera (2048 × 2048 pixels).

Measurements were made blind using NIH ImageJ in control and repeated photostimulated lesions (n=3 and n=5, respectively). We compared these conditions with NAWM corresponding to a non-lesioned *corpus callosum* of mice injected with LPC, but non-photostimulated. G-ratio was calculated by dividing the axon diameter by the total diameter of the axon overlying myelin sheath. Two perpendicular measurements of the largest and shortest diameters per axon were averaged to calculate the g-ratio. To estimate the number of remyelinated axons in each condition, images were divided in four fields and the number of remyelinated axons per field was counted. We considered as remyelinated axons those displaying a low optical density and a g-ratio >0.82 (Supplemental Figure 7
). This value corresponds to the second peak of the g-ratio distribution of control lesions (Figure 4C). To compare the distributions of g-ratio values among conditions, we calculated the g-ratio of at least 300 randomly selected axons per condition.

Statistical Analysis

All data were expressed in mean±SEM. A P value less than 0.05 was considered significant. Since some data sets contained tied values, each data group was subjected to a D'Agostino-Pearson normality test rather than a Shapiro-Wilk test. According to the data structure, two group comparisons were performed using two tailed unpaired Student T-test or Mann-Whitney Test. When data did not fit the assumption of equal variances, a Welch's corrected t-Test was applied. Bonferroni multiple comparisons were used as post-hoc test following one-way and two-way ANOVA or the non-parametric Kruskal–Wallis Test. Data set distributions were compared by using the Kolmogorov-Smirnov distribution Test. Statistics and plotting were performed using GraphPad Prism 5.00 (GraphPad Software Inc., USA), the R environment (48) and Curve Expert 1.4 (Microsoft Corporation) softwares.

Study Approval

All experiments followed European Union and institutional guidelines for the care and use of laboratory animals and were approved by both the French ethical committee for animal care of University Paris Descartes (Paris, France) and the Ministry of National Education and Research (Authorization N° 02015010514019852).

Author Contributions

F.C.O. and C.H. conducted optogenetic, electrophysiological and behavioral experiments, immunostainings and data analysis. M.G. performed EM experiments and analysis, P.Y.H. contributed to initial optogenetic and immunostaining experiments. F.C.O., C.H., and M.C.A. designed experiments. A.N. and B.N.O. assisted in some of the experiment design. All authors wrote the manuscript. M.C.A supervised the project.

Acknowledgments

We thank Manon Omnes for technical assistance and genotyping, the SCM Imaging Platform of the Saints-Pères Biomedical Sciences site of Paris Descartes University for confocal microscopy and the Imaging Platform of the ICM (ICM-Quant) for electron microscopy experiments. We also thank D. Ortolani for her assistance in the initial g-ratio quantification. This work was supported by grants from Fondation pour la Recherche Médicale (FRM, «Equipe FRM DEQ20150331681»), Fondation pour l'aide à la recherche sur la sclérose en plaques (ARSEP) to M.C.A, Agence Nationale pour la Recherche (ANR-14-CE13-0023-02) to M.C.A and B.N.O and from a subaward agreement from the University of Connecticut with funds provided by Grant No. RG-1612-26501 from National Multiple Sclerosis Society (NMSS) to M.C.A. and A.N. Its contents are solely the responsibility of the authors and do not necessarily represent the official views of U.Conn or NMSS. F.C.O. was recipient of a FRM post-doctoral fellowship and is supported by the Chilean National Fund for Scientific and Technological Development (FONDECYT, INICIACION #11160616). F.C.O, C.H. and M.G. were recipients of ARSEP post-doctoral fellowships. M.G. was supported by post-doctoral fellowships the “Investissements d’avenir” ANR-10-IAIHU-06 (IHU-A-ICM) IHU-A-ICM.

References

1. Franklin, R.J.M., Ffrench-Constant, C. Regenerating CNS myelin - from mechanisms to experimental medicines. *Nat Rev Neurosci*. 2017;18(3): 753-769.

2. Chang, A., Tourtellotte, W.W., Rudick, R., Trapp, B.D. Premyelinating oligodendrocytes in chronic lesions of multiple sclerosis. *N Engl J Med*. 2002;346(3): 165-173.

3. Miller, R.H., Mi, S. Dissecting demyelination. *Nat Neurosci*. 2007;10(11): 1351-1354.

4. Barres, B.A., Raff, M.C. Proliferation of oligodendrocyte precursor cells depends on electrical activity in axons. *Nature*. 1993;361(6409): 258-60.

5. Demerens, C., Stankoff, B., Logak, M., Anglade, P., Allinquant, B., Couraud, F., Zalc, B., Lubetzki, C. Induction of myelination in the central nervous system by electrical activity. *Proc Natl Acad Sci U S A*. 1996;93(18): 9887-92.

6. Gibson, E.M., Purger, D., Mount, C.W., Goldstein, A.K., Lin, G.L., Wood, L.S., Inema, I., Miller, S.E., Bieri, G., Zuchero, J.B., Barres, B.A., Woo, P.J., Vogel, H., Monje, M. Neuronal activity promotes oligodendrogenesis and adaptive myelination in the mammalian brain. *Science*. 2014;344(6183): 1252304.

7. Li, Q., Brus-Ramer, M., Martin, J.H., McDonald, J.W. Electrical stimulation of the medullary pyramid promotes proliferation and differentiation of oligodendrocyte progenitor cells in the corticospinal tract of the adult rat. *Neurosci Lett*. 2010;479(2): 128-33.

8 . Mensch, S., Baraban, M., Almeida, R., Czopka, T., Ausborn, J., El Manira, A., Lyons, D.A. Synaptic vesicle release regulates myelin sheath number of individual oligodendrocytes in vivo. *Nat Neurosci*. 2015;18(5): 628-630.

9. Mitew, S., Gobius, I., Fenlon, L.R., McDougall, S.J., Hawkes, D., Xing, Y.L., Bujalka, H., Gundlach, A.L., Richards, L.J., Kilpatrick, T.J., Merson, T.D., Emery, B. Pharmacogenetic stimulation of neuronal activity increases myelination in an axon-specific manner. *Nat Commun*. 2018;9(1): 306.

10. Wake, H., Ortiz, F.C., Woo, D.H., Lee, P.R., Angulo, M.C., Fields, R.D. Nonsynaptic junctions on myelinating glia promote preferential myelination of electrically active axons. *Nat Commun*. 2015;6: 7844.

11. Gautier, H.O.B., Evans, K.A., Volbracht, K., James, R., Sitnikov, S., Lundgaard, I., James, F., Lao-Peregrin, C., Reynolds, R., Franklin, R.J.M., Káradóttir, R.T. Neuronal activity regulates remyelination via glutamate signalling to oligodendrocyte progenitors. *Nat Commun*. 2015;6: 8518.

12. Stevens, B., Tanner, S., Fields, R.D. Control of myelination by specific patterns of neural impulses. *J Neurosci*. 1998;18(22): 9303-9311.

13. Stevens, B., Porta, S., Haak, L.L., Gallo, V., Fields, R.D. Adenosine: a neuron-glial transmitter promoting myelination in the CNS in response to action potentials. *Neuron.* 2002;36(5): 855-868.

14. Nagy, B., Hovhannisyan, A., Barzan, R., Chen, T.-J., Kukley, M. Different patterns of neuronal activity trigger distinct responses of oligodendrocyte precursor cells in the corpus callosum. *PLoS Biol*. 2017;15(8): e2001993.

15. Arenkiel, B.R., Peca, J., Davison, I.G., Feliciano, C., Deisseroth, K., Augustine, G.J., Ehlers, M.D., Feng, G. In vivo light-induced activation of neural circuitry in transgenic mice expressing channelrhodopsin-2. *Neuron*. 2007;54(2): 205-18.

16. Palmer, L.M., Stuart, G.J. Site of action potential initiation in layer 5 pyramidal neurons. *J Neurosci*. 2006;26(6): 1854-1863.

17. Angulo, M.C., Staiger, J.F., Rossier, J., Audinat, E. Distinct local circuits between neocortical pyramidal cells and fast-spiking interneurons in young adult rats. *J Neurophysiol*. 2003;89(2): 943-53.

18. Gensert, J.M., Goldman, J.E. Endogenous progenitors remyelinate demyelinated axons in the adult CNS. *Neuron*. 1997;19(1): 197-203.

19. Sahel, A., Ortiz, F.C., Kerninon, C., Maldonado, P.P., Angulo, M.C., Nait-Oumesmar, B. Alteration of synaptic connectivity of oligodendrocyte precursor cells following demyelination. *Front Cell Neurosci*. 2015;9(): 77.

20. Miron, V.E., Boyd, A., Zhao, J.-W., Yuen, T.J., Ruckh, J.M., Shadrach, J.L., van Wijngaarden, P., Wagers, A.J., Williams, A., Franklin, R.J.M., ffrench-Constant, C. M2 microglia and macrophages drive oligodendrocyte differentiation during CNS remyelination. *Nat Neurosci*. 2013;16(9): 1211-1218.

21. Remaud, S., Ortiz, F.C., Perret-Jeanneret, M., Aigrot, M.-S., Gothié, J.-D., Fekete, C., Kvárta-Papp, Z., Gereben, B., Langui, D., Lubetzki, C., Angulo, M.C., Zalc, B., Demeneix, B. Transient hypothyroidism favors oligodendrocyte generation providing functional remyelination in the adult mouse brain. *eLife*. 2017;6:e29996.

22. Hill, R.A., Patel, K.D., Goncalves, C.M., Grutzendler, J., Nishiyama, A. Modulation of oligodendrocyte generation during a critical temporal window after NG2 cell division. *Nat Neurosci*. 2014;17(11): 1518-1527.

23. Zonouzi, M., Scafidi, J., Li, P., McEllin, B., Edwards, J., Dupree, J.L., Harvey, L., Sun, D., Hübner, C.A., Cull-Candy, S.G., Farrant, M., Gallo, V. GABAergic regulation of cerebellar NG2 cell development is altered in perinatal white matter injury. *Nat Neurosci*. 2015;18(5): 674-682.

24. Hughes, E.G., Orthmann-Murphy, J.L., Langseth, A.J., Bergles, D.E. Myelin remodeling through experience-dependent oligodendrogenesis in the adult somatosensory cortex. *Nat Neurosci*. 2018;21(5): 696-706.

25. Baraban, M., Mensch, S., Lyons, D.A. Adaptive myelination from fish to man. *Brain research*. 2016;1641: 149-161.

26. Wake, H., Lee, P.R., Fields, R.D. Control of local protein synthesis and initial events in myelination by action potentials. *Science*. 2011;333(6049): 1647-1651.

27. Hines, J.H., Ravanelli, A.M., Schwindt, R., Scott, E.K., Appel, B. Neuronal activity biases axon selection for myelination in vivo. *Nat Neurosci*. 2015;18(5): 683-689.

28. Maldonado, P.P., Angulo, M.C. Multiple Modes of Communication between Neurons and Oligodendrocyte Precursor Cells. *Neuroscientist*. 2015;21(3): 266-276.

29. Huang, Y., Dreyfus, C.F. The role of growth factors as a therapeutic approach to demyelinating disease. *Exp Neurol*. 2016;283: 531-40.

30. Lundgaard, I., Luzhynskaya, A., Stockley, J.H., Wang, Z., Evans, K.A., Swire, M., Volbracht, K., Gautier, H.O., Franklin, R.J., Attwell, D., Karadottir, R.T. Neuregulin and BDNF induce a switch to NMDA receptor-dependent myelination by oligodendrocytes. *PLoS Biol*. 2013;11(12): e1001743.

31. Voronova, A., Yuzwa, S.A., Wang, B.S., Zahr, S., Syal, C., Wang, J., Kaplan, D.R., Miller, F.D. Migrating Interneurons Secrete Fractalkine to Promote Oligodendrocyte Formation in the Developing Mammalian Brain. *Neuron*. 2017;94: 500-516.e9.

32. Ishibashi, T., Dakin, K.A., Stevens, B., Lee, P.R., Kozlov, S.V., Stewart, C.L., Fields, R.D. Astrocytes promote myelination in response to electrical impulses. *Neuron*. 2006;49(6): 823-832.

33. Domingues, H.S., Portugal, C.C., Socodato, R., Relvas, J.B. Oligodendrocyte, Astrocyte, and Microglia Crosstalk in Myelin Development, Damage, and Repair. *Front Cell Dev Biol*. 2016;4: 71.

34. Erlanger, J., Gasser, H. The action potential in fibers of slow conduction in spinal roots and somatic nerves. *Am J Physiol*. 1930;92(1): 43-82.

35. Gasser, H., Erlanger, J. The role played by the sizes of the constituent fibers of a nerve trunk in determining the form of its action potential wave. *Am J Physiol*. 1927;80(3): 522-547.

36. Dimou, L., Gallo, V. NG2-glia and their functions in the central nervous system. *Glia*. 2015;63(8): 1429-1451.

37. Green, A.J., Gelfand, J.M., Cree, B.A., Bevan, C., Boscardin, W.J., Mei, F., Inman, J., Arnow, S., Devereux, M., Abounasr, A., Nobuta, H., Zhu, A., Friessen, M., Gerona, R., von Büdingen, H.C., Henry, R.G., Hauser, S.L., Chan, J.R. Clemastine fumarate as a remyelinating therapy for multiple sclerosis (ReBUILD): a randomised, controlled, double-blind, crossover trial. *Lancet*. 2017;390(10111): 2481-2489.

38. Bechler, M.E., Swire, M., Ffrench-Constant, C. Intrinsic and adaptive myelination-A sequential mechanism for smart wiring in the brain. *Dev Neurobiol*. 2018;78(2): 68-79.

39. Abboud, H., Hill, E., Siddiqui, J., Serra, A., Walter, B. Neuromodulation in multiple sclerosis. *Mult Scler*. 2017;23(13): 1663-1676.

40. Berk, C., Carr, J., Sinden, M., Martzke, J., Honey, C.R. Thalamic deep brain stimulation for the treatment of tremor due to multiple sclerosis: a prospective study of tremor and quality of life.. *J Neurosurg*. 2002;97(4): 815-820.

41. Oliveria, S.F., Rodriguez, R.L., Bowers, D., Kantor, D., Hilliard, J.D., Monari, E.H., Scott, B.M., Okun, M.S., Foote, K.D. Safety and efficacy of dual-lead thalamic deep brain stimulation for patients

with treatment-refractory multiple sclerosis tremor: a single-centre, randomised, single-blind, pilot trial. *Lancet*. 2017;16(9): 691-700.

42. Cordella, R., Franzini, A., La Mantia, L., Marras, C., Erbetta, A., Broggi, G. Hypothalamic stimulation for trigeminal neuralgia in multiple sclerosis patients: efficacy on the paroxysmal ophthalmic pain. *Mult Scler*. 2009;15(11): 1322-1328.

43. Centonze, D., Koch, G., Versace, V., Mori, F., Rossi, S., Brusa, L., Grossi, K., Torelli, F., Prosperetti, C., Cervellino, A., Marfia, G.A., Stanzione, P., Marciani, M.G., Boffa, L., Bernardi, G. Repetitive transcranial magnetic stimulation of the motor cortex ameliorates spasticity in multiple sclerosis. *Neurology*. 2007;68(13): 1045-1050.

44. Centonze, D., Petta, F., Versace, V., Rossi, S., Torelli, F., Prosperetti, C., Rossi, S., Marfia, G.A., Bernardi, G., Koch, G., Miano, R., Boffa, L., Finazzi-Agrò, E. Effects of motor cortex rTMS on lower urinary tract dysfunction in multiple sclerosis. *Mult Scler*. 2007;13(2): 269-271.

45. Koch, G., Rossi, S., Prosperetti, C., Codecà, C., Monteleone, F., Petrosini, L., Bernardi, G., Centonze, D. Improvement of hand dexterity following motor cortex rTMS in multiple sclerosis patients with cerebellar impairment. *Mult Scler*. 2008;14(7): 995-998.

46. Palm, U., Ayache, S.S., Padberg, F., Lefaucheur, J.-P. Non-invasive brain stimulation therapy in multiple sclerosis: a review of tDCS, rTMS and ECT results. *Brain Stimul*. 2014;7(6): 849-854.

47. Balia, M., Benamer, N., Angulo, M.C. A specific GABAergic synapse onto oligodendrocyte precursors does not regulate cortical oligodendrogenesis. *Glia*. 2017;65(11): 1821-1832.

48. R Core Team for Statistical Computing, R.F. (Ed.) *R: A language and environment for statistical computing*. R Development Core Team, Vienna, Austria. (2014).

Figures

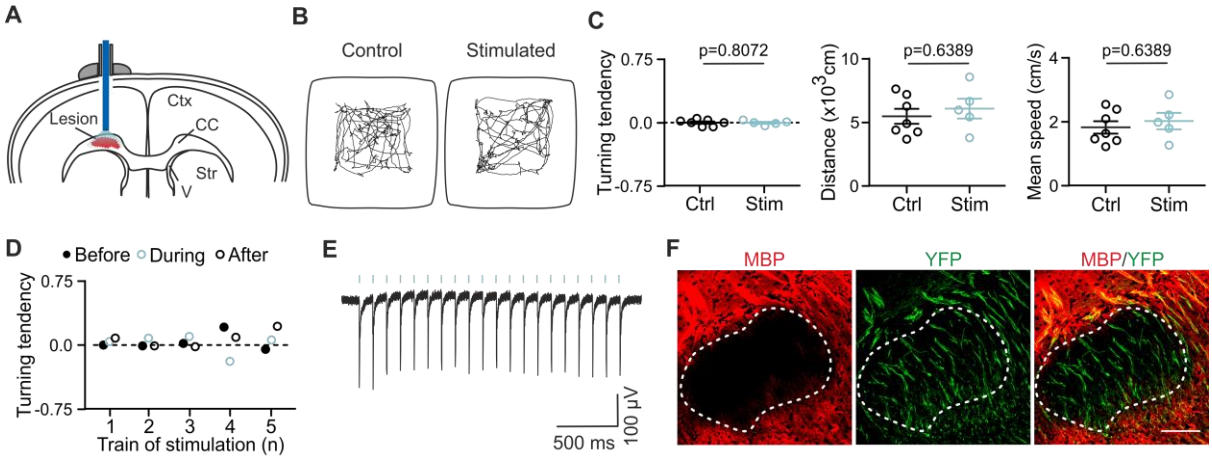

Figure 1. Moderate optogenetic stimulation of channelrhodopsin-2 (ChR2)-expressing demyelinated fibers in vivo

A. Scheme of the optogenetic stimulation of lysophosphatidylcholine (LPC)-induced demyelinated lesions in *corpus callosum (CC)*. The mini-optic fiber is placed above the injected CC (Ctx: cortex, Str: striatum, V: ventricle). **B**. Representative open-field trajectory maps (5 min) of a non-photostimulated mouse (Control) and a photostimulated mouse including the first photostimulation train at 7 dpi (Stimulated; 10 ms light pulses at 20 Hz for 30 s and ~1 mW output; n=7 Controls and n=5 Stimulated mice). **C**. Similar turning tendency, traveled distance and mean speed between controls and photostimulated mice over a 50 min trajectory at 7 dpi for the same mice ($p>0.05$, two-tailed Mann-Whitney Test). **D**. Turning tendency before, during and after photostimulation trains (30 s periods) for a single photostimulated mouse at 7 dpi (n=7 Control and n=5 Stimulated mice). **E**. Local field potential (LFP) evoked by photostimulation (blue bars) inside the demyelinated lesion in an anesthetized mouse (n=13 mice). **F**. Confocal images of a LPC-induced demyelinated lesion

in *corpus callosum* at 7dpi. The lesion (dashed line) is recognized by the lack of myelin basic protein (MBP) staining (red). ChR2-expressing fibers are detected by the expression of YFP (green). Scale bar 100µm.

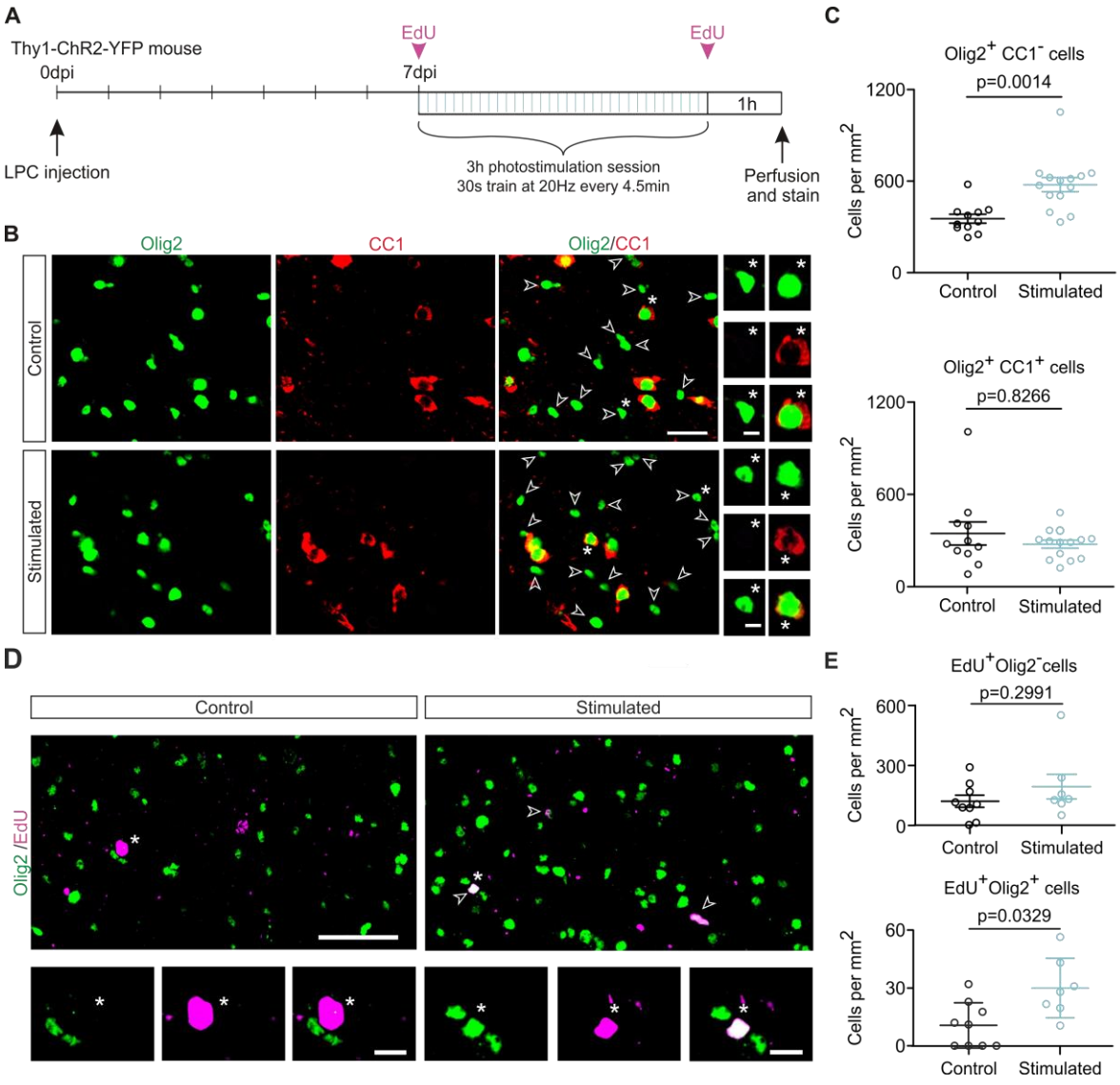

Figure 2. A photostimulation session in vivo increases oligodendrocyte precursor cell (OPC) density in demyelinated lesions

A. Experimental design at 7 dpi with a 3h photostimulation session paradigm. **B**. Olig2 (green) and CC1 (red) cells stained at 7 dpi in control lysophosphatidylcholine (LPC)-induced lesions (control) and after a photostimulation session (stimulated). $Olig2^+/CC1^-$ OPCs are indicated (white arrowheads). Insets: $Olig2^+/CC1^-$ OPCs and $Olig2^+/CC1^+$ oligodendrocytes (OLs) in both conditions. Note that colors are pseudo-colors, and correspond to Alexa-405 (405 nm excitation) for Olig2 and Alexa-633 (633 nm excitation)

for CC1. Scale bars: 25 µm, 5 µm. **C**. Density of $Olig2^{+}/CC1^{-}$ OPCs (left) and $Olig2^{+}/CC1^{+}$ OLs (right) in control and after a photostimulation session at 7 dpi (n=11 and n=14 Control and Stimulated lesions; U= 18.00 and U=72.50, respectively; two tailed Mann-Whitney Test). **D**. Olig2 (green) and 5-Ethynyl-2´-deoxyuridine (EdU; magenta) cells stained at 7 dpi in Control and photostimulated (Stimulated) LPC-induced lesions. Note the presence of $EdU^{+}/Olig2^{+}$ cells (arrowheads) inside the lesions in photostimulated, but not in control lesions (insets). Note that colors are pseudo-colors and correspond to Alexa-405 (405 nm excitation) for Olig2 and Alexa-647 (647 nm excitation) for EdU. Scale bars: 50 µm, 10 µm. **E**. Density of $EdU^{+}/Olig2^{-}$ (top) and $EdU^{+}/Olig2^{+}$ (bottom) cells at 7 dpi (n=9 and n=7 Control and Stimulated lesions; U= 20.00 and U=11.00, respectively; two tailed Mann-Whitney Test).

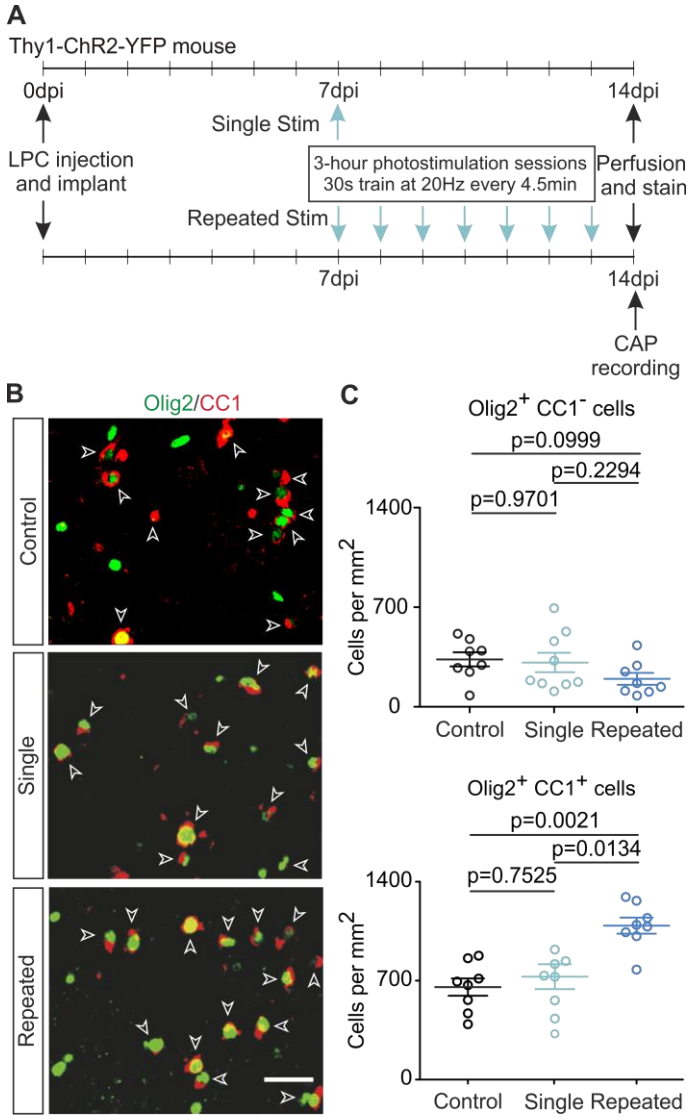

Figure 3. Repeated photostimulation in vivo is required to OPC differentiation in demyelinated lesions

A. Experimental design with a single and repeated photostimulation paradigm during a week. **B**. Olig2 (green) and CC1 (red) cells stained at 14 dpi in control lysophosphatidylcholine (LPC)-induced lesions (Control), after a single photostimulation session at 7 dpi (Single) and after seven photostimulation sessions over a week (Repeated). Mature $Olig2^{+}/CC1^{+}$

oligodendrocytes (OLs) are indicated (white arrowheads). Note that colors are pseudo-colors, and correspond to Alexa-405 (405 nm excitation) for Olig2 and Alexa-633 (633 nm excitation) for CC1. Scale bar: 25 µm. **C**. Density of $Olig2^{+}/CC1^{-}$ OPCs (left) and $Olig2^{+}/CC1^{+}$ OLs (bottom) in the three different conditions at 14 dpi (n=8, n=9 and n=8 lesions for Control, Single and Repeated protocols, respectively; K-W st.=3.69 and K-W st.=11.48, respectively; Kruskal-Wallis Test followed by a Bonferroni's multiple comparison).

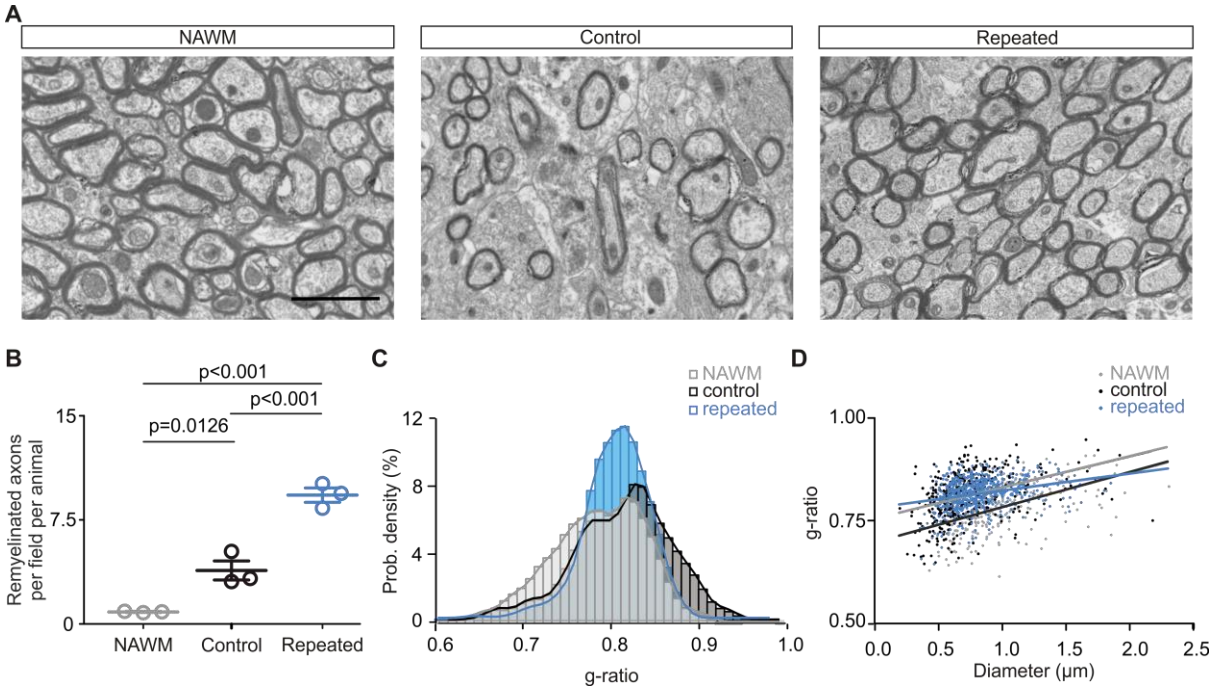

Figure 4. Repeated photostimulation in vivo enhances remyelination

A. Electron micrographs of transversal sections from non-demyelinated *corpus callosum* (normal appearing white matter; NAWM), control lysophosphatidylcholine (LPC)-induced lesions (Control) and after repeated photostimulation of LPC-induced lesions (Repeated) at 14 dpi (n=3 mice per condition). Scale bar: 2 µm. **B.** Dot plot of the average number of remyelinated axons per field per animal for NAWM, Control and Repeated LPC-induced lesions at 14 dpi (n=3 mice per condition; F=73,96, one-way ANOVA test followed by a Bonferroni multiple comparison). **C.** Distribution of g-ratio values per condition (n=302, n=545 and n=812 measured axons for each condition, respectively; D=0.144, p=0.001 for NAWM *vs* control, D=0.238, p=0.001 for NAWM *vs* repeated, D=0.102, p=0.042 for control *vs* repeated; Kolmogorov-Smirnov test). **D.** Scatter plot of the same g-ratio values as a measure of myelin thickness for NAWM (grey), Control (black) and Repeated LPC-induced

lesions (blue) (comparison of slopes: F=9.8643, p=0.687 for NAWM *vs* control and p<0.0001 for both NAWM *vs* repeated and control *vs* repeated; one-way ANOVA test followed by a Bonferroni multiple comparison).

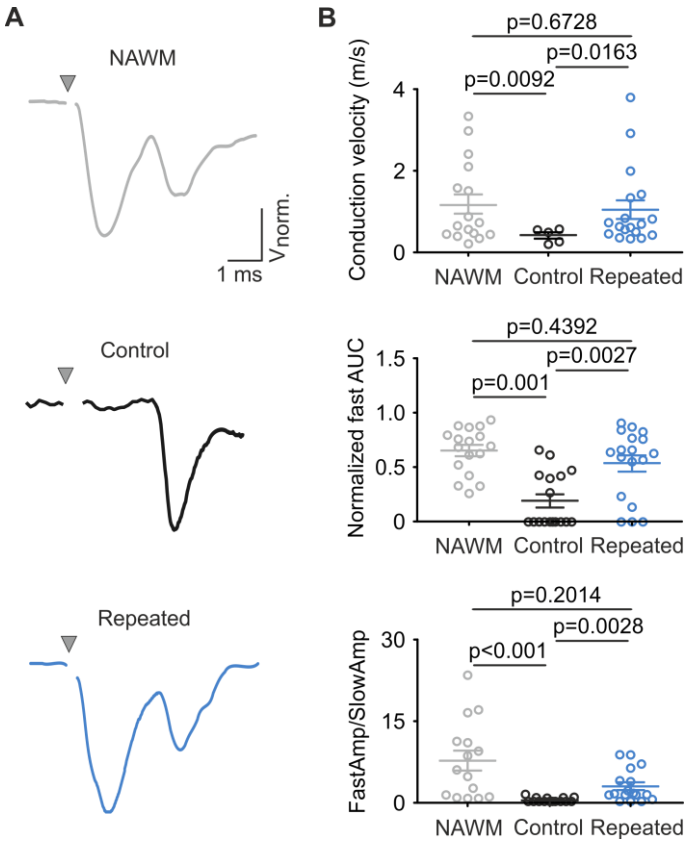

Figure 5. Repeated photostimulation in vivo promotes functional recovery in demyelinated lesions

A. Representative compound action potentials (CAPs) for NAWM, control and repeated photostimulated lesions at 14 dpi. CAPs were obtained after substracting average traces before and after application of 1 µM tetrodotoxin (TTX) (19). Note that the first peak corresponding to myelinated fibers disappeared in control LPC-induced lesions but was rescued after repeated stimulation. The time of stimulation is indicated (grey arrowheads). **B**. Dot plots of conduction velocity (top), normalized area-under-the-curve (AUC; middle) for the fast component and amplitude ratio between fast and slow components of CAPs (fastAmp/slowAmp; bottom). Note that only 5 out of 17 recording in control LPC-induced

lesions had a fast component (n=17 recordings for NAWM and Control, n=18 recordings for Repeated; n=3 mice per condition; W-t st.=0.43 and df =41, W-t st.=2.94 and df =17, W-t st.=2.62 and df =20, respectively, for conduction velocity; Welch's t-corrected test; K-W st.= 18.40 for normalized AUC and K-W st.=20.85 for fastAmp/slowAmp; Kruskal-Wallis Test followed by a Bonferroni's multiple comparison).